Full title: *In vivo* interictal signatures of human periventricular heterotopia.

Running title: Signatures of periventricular heterotopia

Authors: Valerio Frazzini[1,2,3]*, Stephen Whitmarsh[2]*, Katia Lehongre[2], Pierre Yger[4], Bertrand Mathon[2,3,5], Claude Adam[1], Dominique Hasboun[2,3,6], Virginie Lambrecq[1,2,3] and Vincent Navarro[1,2,3]†

[1]AP-HP, Hôpital de la Pitié Salpêtrière, Unité d'Épilepsie and Centre de Référence des Epilepsies rares, F-75013, Paris, France

[2]Institut du Cerveau et de la Moelle épinière, ICM, F-75013, Paris, France

[3]Sorbonne Université, UMR S1127, F-75013, Paris France

[4]Institut de la Vision, INSERM UMRS 968, UPMC UM 80, France

[5]AP-HP, Hôpital de la Pitié Salpêtrière, Département de Neurochirurgie, F-75013, Paris, France

[6]AP-HP, Hôpital de la Pitié Salpêtrière, Département de Neuroradiologie, F-75013, Paris, France

* Contributed equally to this study.

†Corresponding author:

Unité d'Epilepsie, Hôpital Pitié-Salpêtrière,

47 boulevard de l'Hôpital, 75651 Paris cedex 13, France

Tel: 33 1 42 16 19 40, Fax: 33 1 42 16 19 42

E-mail: vincent.navarro@aphp.fr

ORCID: Valerio Frazzini 0000-0003-1187-3352, Stephen Whitmarsh 0000-0002-3969-6565, Pierre Yger 0000-0003-1376-5240, Vincent Navarro 0000-0003-0077-8114

Abstract

Periventricular nodular heterotopia (PNH) is a common cause of drug-resistant epilepsy, characterized by nodules of ectopic neurons adjacent to the lateral ventricles. It remains controversial whether neurons within the nodules generate epileptic activity. In contrast to other types of cortical malformations, no unique interictal patterns have been described in PNH. We report the first multi-level analysis of long-term microelectrode recordings of the interictal activities from three nodules in two epileptic patients during presurgical evaluation. In both patients, seizures originated from the ectopic nodules. Highly consistent interictal activities were identified in all three nodules 1) trains of periodic slow waves (n=2855), 2) isolated slow deflections (n=1631), both with superimposed fast activity, and 3) epileptic spikes (n=6986). Patterns were highly local and largely invisible on the adjacent macro-electrode contacts. Spike analyses showed that the vast majority of units (n=25) were strongly modulated during all interictal patterns. The same units were involved in all three patterns, while showing different patterns of firing rate modulation during the interictal events. These results are consistent with an altered regulation of cellular excitability and suggest that periodic patterns may result from fluctuation in inhibition and rebound excitation in the same neuronal network.

Introduction

Periventricular nodular heterotopia (PNH) is one of the most common types of cortical malformation (Guerrini and Dobyns, 2014). PNH is the result of an abnormal neuronal migration process wherein clusters of neurons form nodular masses of gray matter close to the walls of the lateral ventricles (Dubeau *et al*., 1995). The majority of patients with PNH suffer from focal pharmaco-resistant epilepsy (Battaglia *et al*., 2006), for which neurosurgery can be considered. Stereotactic EEG (sEEG) is often required for pre-surgical evaluation of region to be potentially resected, as seizures might start in PNH, overlying cortex, or both (Kothare *et al*., 1998; Tassi, 2004; Battaglia *et al*., 2006; Valton *et al*., 2008; Mirandola *et al*., 2017). The seizure onset zone (SOZ) can also be inferred from patterns of interictal activity that are known to correlate with specific epileptogenic lesions. For example, patients with type-IIb focal cortical dysplasia frequently show localized periodic or pseudo-periodic spikes or poly-spikes (Palmini *et al*., 1995). In PNH, reports of stereotypical interictal patterns are more limited. One sEEG study found an absence of background activity in PNH, together with low voltage, low frequency activity, frequent high voltage spikes and positive waves (Tassi, 2004), while another study only reported frequent low voltage spikes-and-waves (Mirandola *et al*., 2017). Neurons within the ectopic tissue are disorganized (Dubeau *et al*., 1995), which would limit spatial summation of electric currents and might contribute to the heterogeneity in sEEG findings. Microelectrodes, however, can record local-field-potentials (LFPs) and spikes from nearby (≈ 140µm) neurons, and are therefore less dependent on the spatial summation of current flow (Buzsaki, 2004). Furthermore, recording interictal activity from PNH can evaluate unequivocally the involvement of ectopic neurons rather than surrounding tissues in epileptic activities.

The goal of our study was to identify interictal LFP signatures and the underlying neuronal substrates that originate within the epileptogenic nodules in PNH. Interictal patterns were described on an unprecedented level of microscopic detail by means of microelectrode recordings from three PNH nodules in two patients. LFP patterns were initially identified on the basis of their morphological and pathological features and then described in the time and frequency domains. Single units were extracted using spike-sorting algorithms (Yger *et al*., 2018), after which extracellular spike-width and peak-trough time were used to describe units on the basis of detected morphological and electrophysiological features (Henze *et al*., 2000).

Materials and methods

sEEG recording

Patients gave a written informed consent (project C11-16 conducted by INSERM and approved by the local ethic committee, CPP Paris VI). Two patients were implanted with bilateral intracranial depth electrodes (AdTech®) according to the clinical practice and the epilepsy features of the patients. Two (Patient 1) and three (Patient 2) Behnke-Fried type macro-micro electrodes were inserted (Fried *et al*., 1999). Signals from macro- and microelectrodes were continuously and synchronously recorded at 4kHz and 32kHz, respectively, using a hardware filter at 0.01Hz (Atlas Recording System; NeuraLynx, Tucson, AZ, USA). Post-implantation electrode locations were based on a pre-implantation 3T 3D-MRI, post-implant 1.5T 3D-MRI and CT scan, integrated using the Epiloc toolbox (Pérez-Garcia et al., 2015), an in-house developed plugin for the 3D-Slicer visualization software (Fedorov *et al*., 2012). Macroelectrodes targeting the PNH had two verified contacts as well as microelectrodes placed within the PNH (Table 1).

[Insert Table 1 here]

Visual analysis of micro-LFP patterns

Pathological patterns were identified on the microelectrodes according to traditional morphological characteristics used in clinical practice. Criteria for each pattern were then determined and used for a complete manual scoring of continuous data recorded at the first day after implantation. Patient 1 was analyzed for 24 hours. Patient 2, due to richness of interictal activity, was analyzed for 6 hours. Annotation of data was performed with software developed in-house (MUSE), using single markers for epileptic spikes, and start/end-markers for prolonged patterns and artefacts. Onset and duration of slow waves were determined manually on a subset of annotated patterns. In the case of periodic patterns, only sequences with at least 3 consecutive slow waves were included. Periodicity was determined in accordance with Hirsch *et al*. (2013), by calculating the percentage of slow waves that deviated more than 25% from the average period within each pattern.

Spectral analysis of micro-LFP patterns

Analyses were performed with a combination of FieldTrip (Oostenveld, *et al*., 2011) and custom MATLAB scripts (The Mathworks Inc., Natick, Massachusetts). Time-courses were first aligned according to the max/min peak of filtered data (Supplementary Table 1). Data were then down-sampled to 1kHz. Average LFPs were based on the aligned time-courses. Time–frequency representations (TFRs) were calculated using a Hanning taper applied to an adaptive sliding time window of seven cycles ($t = 7/f$, Δt = 10ms). Average power in 10Hz-200Hz was expressed in percentage change, relative to the baseline-period at −2s to −1s relative to pattern onset. For

epileptic spikes a baseline period of −1s to −0.5s was used, except for the second nodule of Patient 2, where a baseline-period of −2s to −1 s was used due to more extended fluctuations of firing rate preceding the epileptic spike.

Spike sorting and analysis

After selecting electrodes that showed multi-unit activity (MUA), data were temporally whitened, and spikes were automatically detected at 6 median absolute deviations of high-pass filtered (>500Hz) data. Spikes occurring during artefacted periods were ignored. A combination of density-based clustering and template matching algorithms were used to automatically cluster the detected spikes (Yger *et al.*, 2018). Clusters were evaluated on whether they reflected putative single-unit activity (SUA) or multi-unit activity, based on the inter-spike-interval (ISI), the percentage of refractory period violation ($RPV = ISI < 1$ ms) and spike morphology. Resting behavior of detected units were further explored by mean firing rate, Fano factor & Coefficient of Variation (Shinomoto, *et al.*, 2003) and Burst Index (BI) (Constantinidis & Goldman-Rakic, 2002), calculated on the baseline period preceding epileptic spikes to maximize data of consistent resting behavior. Spike-times were epoched and time-locked identically to the LFP analyses. Average spike rates were calculated continuously at 1000Hz, using a Gaussian smoothing kernel of 12.5ms for Epileptic Spikes, and 50ms for the longer patterns to better capture slower modulation in firing rate. Correlations between average time-locked spike-rates of each unit, and the average time-locked LFP of every pattern, were calculated. Finally, spike-rates of each trial were binned into 200 bins for statistical analyses. To control for multiple comparisons and non-normal distributions of firing-rates, we performed non-parametric cluster-based permutation tests (Maris & Oostenveld, 2007) to determine time-periods where firing-rates changed significantly

from baseline. A threshold of $p < 0.01$ (first-level t-test) was used to determine contiguous clusters, after which a threshold of $p < 0.05$ (one-sided correction) determined whether the clusters (sum of t-values) could be explained under permutation ($n = 1000$). Finally, an exploratory classification of detected units into putative pyramidal and interneurons, was based on the half-width duration and trough-peak time of their waveforms (Bartho *et al.*, 2004).

Results

Novel LFP epileptic activities revealed by microelectrodes

In both patients, seizures started at electrode contacts located in the PNH, with a secondary propagation in other cortical areas (Fig. 1J, K & Supplementary patient information). Importantly, we identified three interictal patterns that were consistently found in the nodules (Fig. 1 & 2). These patterns were rarely visible on the macro-electrodes. In fact, epoch-by-epoch correlations between the microelectrode and adjacent macroelectrode contacts showed that the interictal patterns were only present in the most profound macro contact, i.e. within the PNHs (Fig. 2 E).

[Insert Figure 1 and Figure 2 here]

Periodic Slow Waves

Periodic Slow Waves (PSW; Fig.1 C&F, right) were seen in both Nodule 1 (n=1882) and Nodule 2 (n=973). The periodicity of the PSW was clear in the average LFP of Nodule 1 (Fig. 2A, right) and Nodule 2 (Fig. 2B, right). Average ($\pm\sigma$) duration of a single slow wave was 283 ± 74ms in Nodule 1, and 271 ± 72ms in Nodule 2. Time periods between onset of two slow waves was 511

± 148ms in Nodule 1, and 574 ± 152ms in Nodule 2. 83% (Nodule 1, subset *n* = 181) and 79% (Nodule 2, subset *n* = 153) of these time periods varied less than 25% from the average period, in accordance with *periodicity*. Low voltage fast activity (FA) was superimposed on the slow waves. (Fig. 1C&F). Frequency analysis showed a mean peak at 112 Hz (Nodule 1) and 137Hz (Nodule 2). These FA were clearly modulated in accordance with the periodicity of the slow waves.

Fast Activity

Isolated trains of Fast Activity (FA) were seen in both Nodule 1 (n=1005) and 2 (n=93). In Nodule 1, FA was usually superimposed on a polyphasic slow deflection (0.5s-1s, Fig. 1C, middle), while in Nodule 2, FA occurred at the onset of a sharply appearing slow deflection (2s-4s, Fig. 1F, middle). Time-frequency analysis showed that in Nodule 1, power increased to 43Hz and 96Hz for ≈ 0.5s during the FA (Fig. 2A, middle). Nodule 2 showed a clear narrow-band increase of power at 112Hz for at least 1s, (Fig. 2B, middle). These events were isolated, with no tendency to ictal organization. In Nodule 3, low amplitude deflections coincided with periodic short trains of fast activity (n=533), that lasted for 326 ± 79ms. Periods were 1075 ± 241ms (Fig. 1F), of which 91% varied less than 25% (subset *n* = 155) in accordance with *periodicity*. Time-frequency analysis showed clear periodic modulation of high frequency power, centered on 110Hz (Fig. 2D, right).

Epileptic Spikes

Epileptic Spikes (ES) were identified in all three nodules. Nodule 1 (*n*=3878) showed isolated sharp monophasic waves (Fig. 1C, left). In Nodule 2 (*n*=2705), spikes were generally followed (and often preceded) by a slow wave (Fig. 1F, left), which was also apparent in the average time-

locked LFP (Fig. 2B, left). In Nodule 3 (*n*=403), spikes were characterized by a low amplitude di- or triphasic wave (Fig. 1I, left). Low voltage FA was superimposed on ES, with a mean peak at 113Hz, 137Hz and 126Hz, respectively (Fig. 2A-C, left).

[Insert Table 2 here]

Massive neuronal recruitment by interictal patterns

Twenty-one microwires were included in the analysis (Nodule 1: *n*=6, Nodule 2: *n*=7, Nodule 3: *n*=8). Spike clustering resulted in 25 units (Table 2, Fig. 4A) of which 8 (32%) were classified as single units. Single units were shown to significantly modulate their firing rates in response to all interictal patterns. Firing-rate increased up to 505% for PSW, 4281% for FA, and 3840% for ES (Table 2: ↑). Most of the units also showed brief episodes of decreased firing rate surrounding the interictal activities, often by ≈ 100%, i.e. silence (Table 2: ↓; Fig. 2 and Fig. 3A-C). Especially during ES, firing rates strongly decreased in all units within ≈ 500ms surrounding the discharge. Furthermore, trial-by-trial correlations showed that the modulation of firing rates was highly consistent with the timing and shape of the interictal LFP in all units (Table 2; see also: Fig. 2, Fig. 3A-C). A massive increase of firing rate was shown for the very short duration of the ES, while FA was associated with a more prolonged increase of firing rate. During PSW, firing rates showed regular increases and decreases. Interestingly, three clusters, including 2 putative single units, significantly modulated their firing-rate inversely with respect to the interictal LFPs (Fig. 2C: middle panel; Table 2: Nodule 2, Unit 4&5, and Nodule 3, Unit 2).

[Insert Figure 3 here]

Exploratory classification of neuronal types

An exploratory classification of single units into neuronal types was based on the half-width and trough-to-peak time of the action-potential (Fig. 4A). Values separating putative inter-neurons from pyramidal cells were consistent with previous reports (Trough-to-peak: ≈ 0.5ms, Half-amplitude duration: ≈ 0.25ms; Bartho *et al*., 2004). Seven out of 8 units were classified as putative pyramidal cells, while one was consistent with a narrow-spiking putative interneuron (Fig. 4A). No clear differences were observed in firing behavior, although the interneuron did show the highest Fano Factor (Fig. 4 B).

[Insert Figure 4 here]

Discussion

Two highly distinct and consistent interictal LFP patterns were identified within the PNH: Periodic Slow Waves and isolated slow waves with Fast Activity (FA). Heterotopic neurons have been found to be more excitable as result of a deficient A-type potassium currents (Castro, *et al.*, 2001), while NR2A and NR2B subunit expression and regulatory molecular machinery are reduced in preclinical rat models (Colacitti *et al*., 1999) and resected human PNH tissue (Finardi *et al*., 2006). Moreover, a previous *in vitro* study found a dramatic increase in inhibitory GABAergic synaptic transmission of heterotopic neurons (Kitaura *et al*., 2012), which could reflect a compensating drive against the otherwise hyper-excitability of the pathological network of PNH (Calcagnotto, *et al.*, 2002). Our findings are in line with such a hyper-synchronous and hyper-excitable neuronal population.

All interictal patterns were shown to be highly local, and very likely originated within the PNH due to several reasons. First, the cerebral volume explored by microelectrodes is exceedingly small (Buzsaki, 2004). Secondly, the LFP patterns correlated positively only with neighboring macro contacts that were also located within the PNH. Strikingly, all units responded to all interictal patterns, suggesting that the same neuronal population generates the different interictal patterns. Although tentative, we found evidence for both putative pyramidal cells and interneurons, in accordance with histological studies showing both excitatory neurons and interneurons in human PNH (Thom, *et al.*, 2004; Meroni *et al.*, 2009). Neuronal types did not distinguish between interictal patterns, however. Specific network conditions might therefore be more important in determining which interictal pattern will occur at a particular point in time. Periodic patterns might result from alternating inhibition and rebound excitation in the same neuronal network. Different dynamics of the rebound excitation could also result in different LFP patterns. In our data, the increase in firing rate during FA was more sustained than in the other patterns, while preceding decreases in firing rate were more ambiguous. In contrast, epileptic spikes were associated with shorter increases in firing rates, and were clearly surrounded by strong synchronous decreases across a majority of units.

This study presents the first *in vivo* multi-level description of local PNH networks in humans and their organization into multiple epileptic neurophysiological patterns. Previous microelectrode studies have shown strong heterogeneity in neuronal firing during cortical and mesial temporal interictal discharges (Le Van Quyen *et al.*, 2008; Keller *et al.*, 2010; Alvarado-Rojas *et al.*, 2013). In contrary, our findings show highly consistent behavior of units during interictal patterns. This difference might have resulted from the fact that our recordings targeted the PNH

tissue precisely, while the previous studies used an approach that combined various cortical regions and cerebral lesions.

To conclude, our findings show consistent and specific signatures of PNH that can inform future clinical diagnosis, and provide insights into the epileptic mechanisms in patients with PNH. Future research will need to determine whether these signatures can also be found in sub-cortical heterotopia or other types of cortical malformations.

Acknowledgements

We would like to thanks Pierre Pouget (ICM, Pitié-Salpêtrière hospital, Paris, France) for the helpful discussions and comments on the manuscript.

Funding

This study was supported by the program “Investissements d’avenir” ANR-10-IAIHU-06, and grants from the OCIRP-ICM and the Fondation de l’APHP pour la Recherche - Marie-Laure PLV Merchandising.

Competing interests

The authors report no competing interests.

Figure descriptions

Figure 1. *Patient implantation and their LFP patterns.* (A, D and G) Brain MRI showing the electrodes trajectory and the three analyzed nodules (A, Patient 1, nodule 1; B and C, Patient 2, Nodule 2 and 3 respectively). (B, E and H) schematic representation of the used macro-microelectrodes (M1-M5: macroelectrode contacts; u1-u8: microelectrodes). All the geometrical features of the electrodes are expressed in millimeters. Macroelectrode recordings are shown in bipolar montage. In nodule 1 (C) and 2 (F), three LFP patterns were recorded (Epileptic Spikes, Fast Activity, Periodic Slow Wave). These patterns were apparent on microelectrodes (LFP u1 and LFP u2), and to a smaller degree on macroelectrodes (M1-M2). LFP patterns were associated with MUA recorded on the microelectrodes. In nodule 3, two patterns were identified (I) that were apparent on the micro LFP, and to a smaller degree on macro LFPs. (J,K) Examples of a seizure in Patient 1 and 2, showing seizure onset at deep electrode contact and microelectrodes located in periventricular nodules (* on time-axis denotes end of seizure in Patient 1)

Figure 2. *Time-locked LFP and spike analysis.* Spike analysis shows similarities in pathological patterns between PNH nodules (columns), and involvement of the same neuron in all patterns within nodules (rows). Top row in A-D shows average time-locked LFPs of patterns superimposed on average time-resolved spectrum. Middle row in A-D shows rasterplots of spike times, time-locked to the patterns. Bottom row in A-D shows corresponding firing-rates, with clusters of significant change (yellow=increase, blue-decrease), compared to baseline (arrow). E) Correlations between micro (LFP) and macro (LFP) contacts (bipolar reference), showing strongest (positive = yellow) correlation with contacts closest to microelectrode (marker-size =

Pearson's ρ). Negative correlations (blue) show inversion of dipoles for more superficial macroelectrode contacts. Size of markers scale with correlation (ρ).

Figure 3. *Description of single unit behaviour*. Description of single unit behaviour for Nodule 1 (A), Nodule 2 (B), and Nodule 3 (C), including template waveform, ISI histogram of inter-spike-interval and firing-rates time-locked to epileptic patterns, respectively. Significant increases and decreases in firing-rate compared to baseline are indicated in yellow and blue, respectively. D) Description of unit behaviour, including both SUA (filled), and MUA (empty).

Figure 4. *Unit classification.* A) Trough-to-peak plotted against half-amplitude duration, resulting in two clusters of neuronal types. Pyramidal cells cluster on the top right cluster, interneurons on the bottom-left. Empty symbols indicate putative SUA, filled circus putative MUA. Average waveforms and 1000 overlaid responses show putative pyramidal cell (upside-down pyramid shape), and putative narrow-spiking inter-neuron (asterisk).

References

Alvarado-Rojas, C., Lehongre, K., Bagdasaryan, J., Bragin, A., Staba, R., Engel, J., Le Van Quyen, M., *et al.* (2013). Single-unit activities during epileptic discharges in the human hippocampal formation. *Frontiers in Computational Neuroscience*, *7*, 140. doi: 10.3389 /fncom. 2013.00140

Bartho, P., Hirase, H., Monconduit, L., Zugaro, M., Harris, K. D., & Buzsaki, G. (2004). Characterization of Neocortical Principal Cells and Interneurons by Network Interactions and Extracellular Features. *Journal of Neurophysiology*, *92*(1), 600–608. Retrieved 2018-09-26, from http://www.physiology.org/doi/10.1152/jn.01170.2003 doi: 10.1152/jn.01170.2003

Battaglia, G., Chiapparini, L., Franceschetti, S., Freri, E., Tassi, L., Bassanini, S., Granata, T., *et al.* (2006). Periventricular Nodular Heterotopia: Classification, Epileptic History, and Genesis of Epileptic Discharges. *Epilepsia*, *47*(1), 86–97. doi:10.1111/j.1528-1167.2006.00374 .x

Buzsaki, G. (2004). Large-scale recording of neuronal ensembles. *Nature Neuroscience*, *7*(5), 446–451. doi: 10.1038 /nn 1233

Calcagnotto, M. E., Paredes, M. F., & Baraban, S. C. (2002). Heterotopic neurons with altered inhibitory synaptic function in an animal model of malformation-associated epilepsy. *The Journal of Neuroscience: The Official Journal of the Society for Neuroscience*, *22*(17), 7596–7605.

Castro, P. A., Cooper, E. C., Lowenstein, D. H., & Baraban, S. C. (2001). Hippocampal heterotopia lack functional Kv4.2 potassium channels in the methylazoxymethanol model of

cortical malformations and epilepsy. *The Journal of Neuroscience: The Official Journal of the Society for Neuroscience*, *21*(17), 6626–6634.

Colacitti, C., Sancini, G., DeBiasi, S., Franceschetti, S., Caputi, A., Frassoni, C., Battaglia, G., *et al.* (1999). Prenatal methylazoxymethanol treatment in rats produces brain abnormalities with morphological similarities to human developmental brain dysgeneses. *Journal of Neuropathology and Experimental Neurology*, *58*(1), 92–106. doi: 10.1097/00005072-199901000-00010

Constantinidis, C., & Goldman-Rakic, P. S. (2002). Correlated Discharges Among Putative Pyramidal Neurons and Interneurons in the Primate Prefrontal Cortex. *Journal of Neurophysiology*, *88*(6), 3487–3497. doi: 10.1152/jn.00188.2002

Dubeau, F., Tampieri, D., Lee, N., Andermann, E., Carpenter, S., Leblanc, R., Andermann, F., *et al.* (1995). Periventricular and subcortical nodular heterotopia A study of 33 patients. *Brain*, *118*(5), 1273–1287. doi: 10.1093 /brain/ 118.5.1273

Fedorov, A., Beichel, R., Kalpathy-Cramer, J., Finet, J., Fillion-Robin, J.-C., Pujol, S., Kikinis, R., *et al.* (2012). 3d Slicer as an image computing platform for the Quantitative Imaging Network. *Magnetic Resonance Imaging*, *30*(9), 1323–1341. doi: 10.1016 /j.mri. 2012.05.001

Finardi, A., Gardoni, F., Bassanini, S., Lasio, G., Cossu, M., Tassi, L., Battaglia, G., *et al.* (2006). NMDA receptor composition differs among anatomically diverse malformations of cortical development. *Journal of Neuropathology and Experimental Neurology*, *65*(9), 883–893. doi: 10.1097/01 .jnen.0000235117.67558.6d

Fried, I., Wilson, C. L., Maidment, N. T., Engel, J., Behnke, E., Fields, T. A., Ackerson, L. *et al.*, (1999). Cerebral microdialysis combined with single-neuron and electroencephalographic recording in neurosurgical patients. Technical note. *Journal of Neurosurgery*, *91*(4), 697–705. doi: 10.3171/jns.1999.91.4.0697

Guerrini, R., & Dobyns, W. B. (2014). Malformations of cortical development: clinical features and genetic causes. *The Lancet Neurology*, *13*(7), 710–726. doi: 10.1016/S14744422(14)70040-7

Henze, D. A., Borhegyi, Z., Csicsvari, J., Mamiya, A., Harris, K. D., & Buzsaki, G. (2000). Intracellular Features Predicted by Extracellular Recordings in the Hippocampus In Vivo. *Journal of Neurophysiology*, *84*(1), 390–400. doi: 10.1152/jn.2000.84.1.390

Hirsch, L. J., LaRoche, S. M., Gaspard, N., Gerard, E., Svoronos, A., Herman, S. T., Drislane, F. W., *et al.* (2013). American Clinical Neurophysiology Society's Standardized Critical Care EEG Terminology: 2012 version. *Journal of Clinical Neurophysiology*, *30*(1), 27.

Keller, C. J., Truccolo, W., Gale, J. T., Eskandar, E., Thesen, T., Carlson, C., Cash, S., et al. (2010). Heterogeneous neuronal firing patterns during interictal epileptiform discharges in the human cortex. *Brain*, *133*(6), 1668–1681. doi: 10.1093 /brain/awq 112

Kitaura, H., Oishi, M., Takei, N., Fu, Y.-J., Hiraishi, T., Fukuda, M., Kakita, A., *et al.* (2012). Periventricular nodular heterotopia functionally couples with the overlying hippocampus: Optical Imaging of PVNH. *Epilepsia*, *53*(7), e127–e131. doi: 10.1111/j.15281167.2012.03509 .x

Kothare, S. V., VanLandingham, K., Armon, C., Luther, J. S., Friedman, A., & Radtke, R. A. (1998). Seizure onset from periventricular nodular heterotopias: Depth-electrode study. *Neurology*, *51*(6), 1723–1727. doi: 10.1212 /WNL. 51.6.1723

Le Van Quyen, M., Bragin, A., Staba, R., Crepon, B., Wilson, C. L., & Engel, J. (2008). Cell type-specific firing during ripple oscillations in the hippocampal formation of humans. *The Journal of Neuroscience: The Official Journal of the Society for Neuroscience*, *28*(24), 6104–6110. doi: 10.1523 /JNEUROSCI. 0437-08.2008

Maris, E., & Oostenveld, R. (2007). Nonparametric statistical testing of EEG- and MEG-data. *Journal of Neuroscience Methods*, *164*(1), 177–190. doi: 10.1016 /j.jneumeth. 2007.03.024

Meroni, A., Galli, C., Bramerio, M., Tassi, L., Colombo, N., Cossu, M., ... Spreafico, R. (2009). Nodular heterotopia: A neuropathological study of 24 patients undergoing surgery for drug-resistant epilepsy. *Epilepsia*, *50*(1), 116–124. doi: 10.1111/j.15281167.2008.01717 .x

Mirandola, L., Mai, R. F., Francione, S., Pelliccia, V., Gozzo, F., Sartori, I., ... Tassi, L. (2017). Stereo-EEG: Diagnostic and therapeutic tool for periventricular nodular heterotopia epilepsies. *Epilepsia*, *58*(11), 1962–1971. doi: 10.1111 /epi. 13895

Oostenveld, R., Fries, P., Maris, E., & Schoffelen, J.-M. (2011). FieldTrip: Open Source Software for Advanced Analysis of MEG, EEG, and Invasive Electrophysiological Data. *Computational Intelligence and Neuroscience*, *2011*, 1–9. doi: 10.1155/2011/156869

Palmini, A., Gambardella, A., Andermann, F., Dubeau, F., da Costa, J. C., Olivier, A., ... Kim, H.I. (1995, April). Intrinsic epileptogenicity of human dysplastic cortex as suggested by corticography and surgical results. *Annals of Neurology*, *37*(4), 476–487. doi: 10.1002 /ana. 410370410

Pérez-García F., Lehongre K., Bardinet E., Jannin P., Navarro V., Hasboun D., Fernandez-Vidal S. 2015. Automatic segmentation of depth electrodes implanted in epileptic patients: a modular

tool adaptable to multicentric protocols. 31st International Epilepsy Congress. (https://icm-institute.org/fr/cenir-stim-stereotaxy-core-facility-techniques-images-models/)

Shinomoto, S., Shima, K., & Tanji, J. (2003). Differences in spiking patterns among cortical neurons. *Neural Computation*, *15*(12), 2823–2842. doi: 10.1162/089976603322518759

Tassi, L. (2004). Electroclinical, MRI and neuropathological study of 10 patients with nodular heterotopia, with surgical outcomes. *Brain*, *128*(2), 321–337. doi: 10.1093 /brain/awh 357

Thom, M., Martinian, L., Parnavelas, J. G., & Sisodiya, S. M. (2004, August). Distribution of Cortical Interneurons in Grey Matter Heterotopia in Patients with Epilepsy. *Epilepsia*, *45*(8), 916–923. doi: 10.1111/j.00139580.2004.46603 .x

Valton, L., Guye, M., McGonigal, A., Marquis, P., Wendling, F., R´egis, J., Bartolomei, F., *et al.* (2008). Functional interactions in brain networks underlying epileptic seizures in bilateral diffuse periventricular heterotopia. *Clinical Neurophysiology*, *119*(1), 212–223. doi: bartho

Yger, P., Spampinato, G. L., Esposito, E., Lefebvre, B., Deny, S., Gardella, C., Marre, O. *et al.* (2018). A spike sorting toolbox for up to thousands of electrodes validated with ground truth recordings in vitro and in vivo. *eLife*, *7*. doi: 10.7554 /eLife. 34518

		Macro contacts							
N	Micro	1	2	3	4	5	6	7	8
1 (R)	GM PNH	GM PNH	GM PNH *lat*	GM STS	GM STS	GM STS	GM SMG	GM SMG	XC
2 (R)	GM PNH	GM PNH	GM PNH *lat*	WM	GM STG	GM STS *T2*	GM STS *T2*	GM *T2*	GM *T2*
3 (L)	GM PNH	GM PNH *im*	GM PNH *im*	LTO	LTO *T3*	WM	WM	GM/WM *T3*	GM *T3*

Table 1. *Localization of electrode contacts.* N = Nodule, L = Left, R = Right hemisphere, PNH = Periventricular Heterotopic Nodule, GM = Grey matter, WM = White matter, *lat* = lateral, *im* = inferior medial, LTO = Lateral Temporo-Occipital Sulcus, SMG = SupraMarginal Gyrus, STS = Superior Temporal Sulcus, *T2* = Middle Temporal Gyrus, *T3* = Inferior Temporal Gyrus.

				Epileptic Spike			Fast Activity			Periodic Slow Wave			
N	ID	#	RPV	↑	↓	ρ	↑	↓	ρ	↑	↓	ρ	F
1	2	35402	0.09	3840‡	95‡	0.68‡	406‡	83‡	0.63‡	355‡	82‡	0.79‡	A
	7	35603	0.03	285‡	98‡	0.50‡	493‡	69‡	0.68‡	128‡	76‡	0.70‡	
	1	324414	3.32	373‡	69‡	0.74‡	319‡	48‡	0.54‡	153‡	54‡	0.84‡	
	3	59035	0.77	2421‡	84‡	0.66‡	238‡	58‡	0.60‡	180‡	71‡	0.82‡	
	4	9032	0.43	3074‡	100‡	0.75‡	361‡	96‡	0.47‡	201‡	81‡	0.80‡	
	5	75177	1.48	1575‡	65‡	0.90‡	249‡	63‡	0.54‡	305‡	61‡	0.88‡	
	6	28386	0.72	1144‡	97‡	0.72‡	468‡	79‡	0.69‡	216‡	66‡	0.66‡	

				Epileptic Spike			Fast Activity			Periodic Slow Wave			
N	ID	#	RPV	↑	↓	ρ	↑	↓	ρ	↑	↓	ρ	F
2	5	177686	0.90	24‡	91‡	-0.45‡	n.s.	93‡	-0.68‡	22‡	26‡	-0.68‡	C
	8	22797	0.67	1582‡	97‡	0.67‡	4281	100*	0.86‡	505‡	98‡	0.83‡	
	1	6523	0.14	524‡	100‡	0.44‡	n.s.	n.s.	0.07‡	170‡	n.s.	0.43‡	
	2	11431	0.45	599‡	96‡	0.45‡	n.s.	100†	0.09‡	105‡	60*	0.39‡	
	3	92917	1.78	1058‡	99‡	0.59‡	646‡	100‡	0.53‡	392‡	91‡	0.56‡	
	4	20365	0.56	n.s.	60‡	-0.16‡	n.s.	100‡	-0.29‡	n.s.	n.s.	-0.26‡	
	6	56998	0.57	40‡	52‡	0.28‡	n.s.	n.s.	n.s.	n.s.	n.s	0.24‡	
	7	15479	2.47	900‡	89‡	0.71‡	1536	100†	0.85‡	231‡	60‡	0.75‡	B
	9	79082	3.36	744‡	97‡	0.80‡	1484	100‡	0.69‡	264‡	87‡	0.74‡	
	10	156754	2.52	153‡	78‡	0.64‡	118‡	73†	0.49‡	35†	39‡	0.44‡	

				Epileptic Spike			Periodic Fast Activity						
N	ID	#	RPV	↑	↓	ρ	↑	↓	ρ				F
3	2	24774	0.48	1905‡	100‡	-0.12‡	297‡	98‡	0.70‡				
	4	5020	0.02	n.s.	100‡	0.39‡	588*	100‡	0.65‡				
	5	4429	0.00	1968*	100‡	0.49‡	467*	100‡	0.66‡				
	7	13844	0.14	1825*	100‡	0.05*	543‡	100‡	0.67‡				D
	1	103242	3.87	1796‡	96‡	0.36‡	181‡	91‡	0.74‡				
	3	43938	1.33	1153‡	99‡	0.37‡	291‡	93‡	0.50‡				
	6	23329	0.90	1042‡	94‡	0.26‡	267‡	78‡	0.78‡				
	8	11527	0.65	1232*	100‡	0.05*	465‡	100‡	0.75‡				

Table 2. *Spike analysis summary.* N = Nodule, ID = unit, # = number of action potentials. Increases (↑) and decreases (↓) in firing-rate of % baseline, for most significant temporal cluster (*n.s.* = non-significant), ρ = Pearson correlation between spike-rate and LFP. F2 = Panel of Figure 2 for more detailed presentation of cell behavior. Single units are highlighted in gray (see also Figure 4). $* = p < 0.025$, † = $p < 0.01$, ‡ = $p < 0.001$.

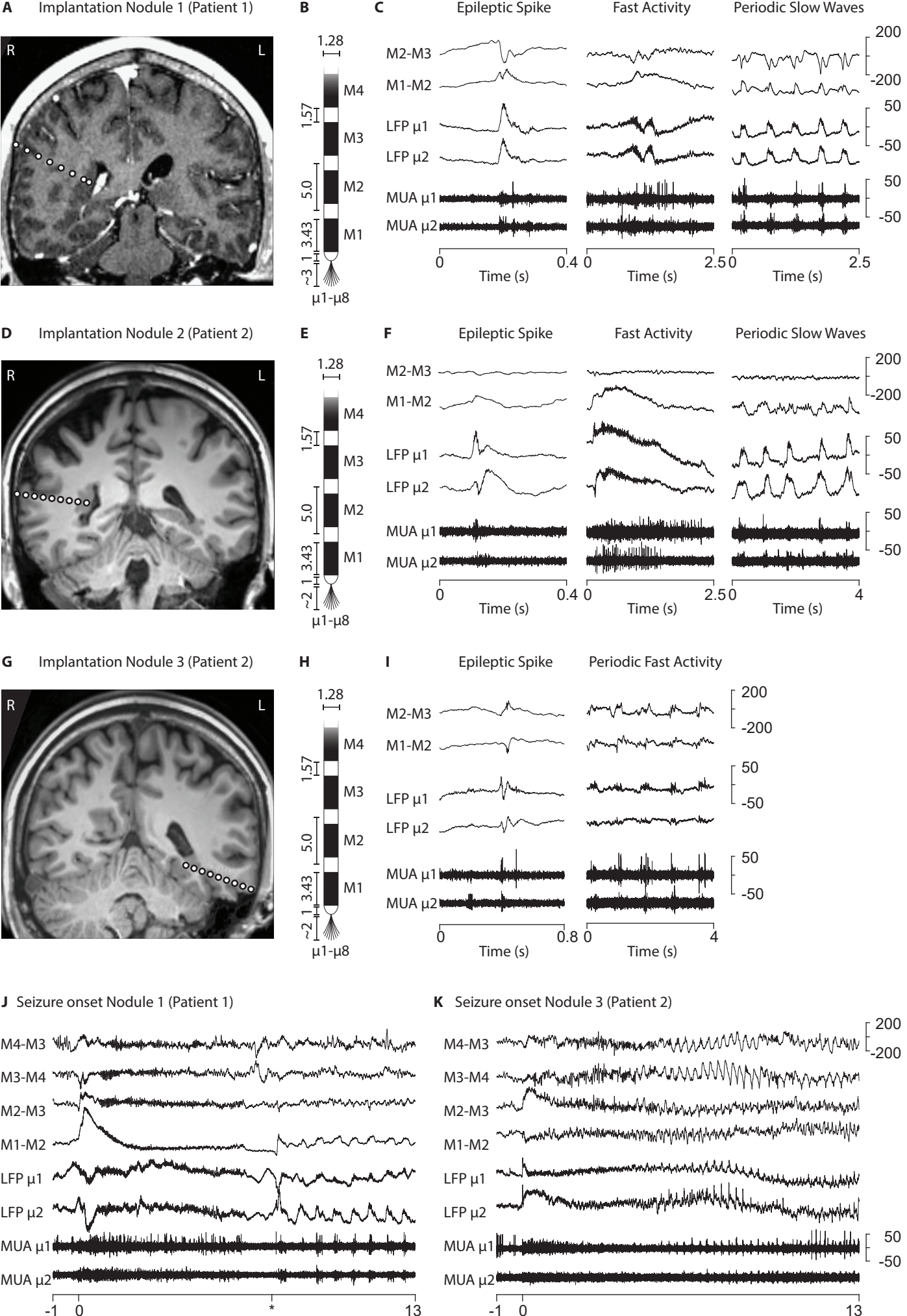
A
Implantation Nodule 1 (Patient 1)
R
L
B
1.28
M4
1.57
M3
M2
5.0
M1
3.43
1
~3
μ1-μ8
C
Epileptic Spike
Fast Activity
Periodic Slow Waves
M2-M3
M1-M2
LFP μ1
LFP μ2
MUA μ1
MUA μ2
200
-200
50
-50
0
0.4
2.5
Time (s)
D
Implantation Nodule 2 (Patient 2)
E
F
4
G
Implantation Nodule 3 (Patient 2)
H
I
Periodic Fast Activity
0.8
J
Seizure onset Nodule 1 (Patient 1)
M4-M3
M3-M4
-1
*
13
K
Seizure onset Nodule 3 (Patient 2)

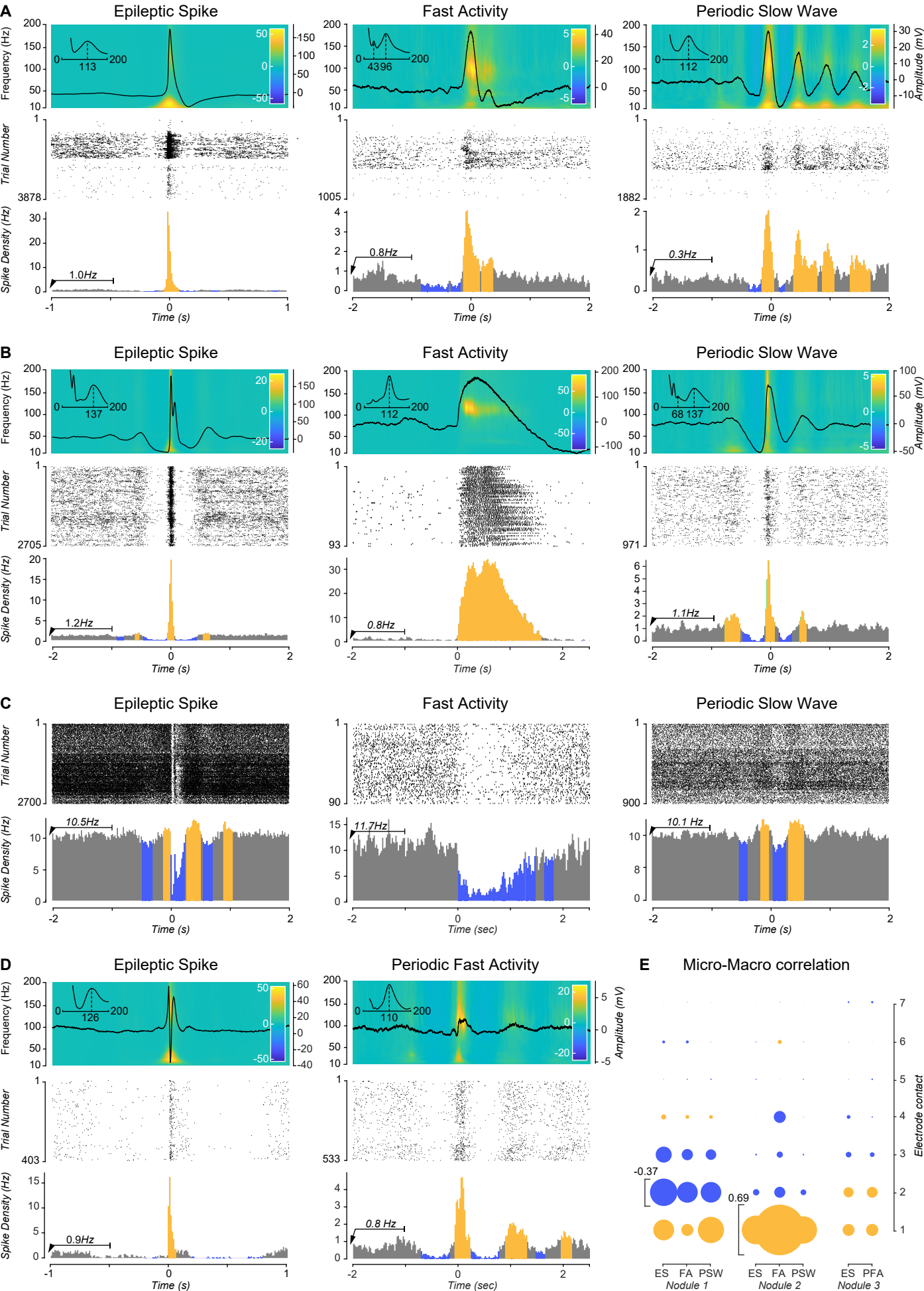
A
Epileptic Spike
Fast Activity
Periodic Slow Wave
Frequency (Hz)
Amplitude (mV)
Trial Number
Spike Density (Hz)
1.0Hz
0.8Hz
0.3Hz
Time (s)
B
Epileptic Spike
Fast Activity
Periodic Slow Wave
1.2Hz
0.8Hz
1.1Hz
C
Epileptic Spike
Fast Activity
Periodic Slow Wave
10.5Hz
11.7Hz
10.1 Hz
Time (sec)
D
Epileptic Spike
Periodic Fast Activity
0.9Hz
0.8 Hz
E
Micro-Macro correlation
Electrode contact
-0.37
0.69
ES FA PSW
Nodule 1
ES FA PSW
Nodule 2
ES PFA
Nodule 3

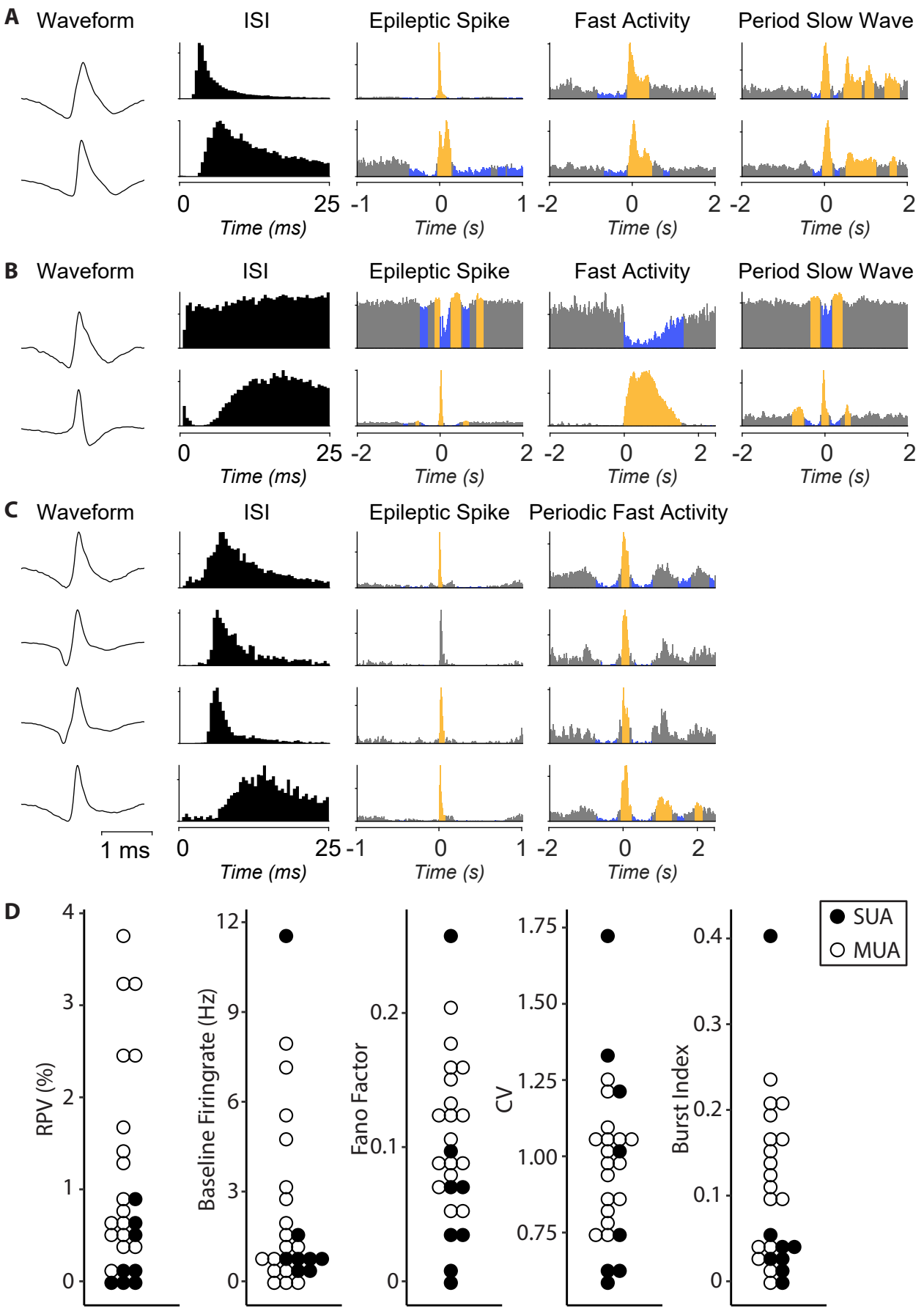
A
Waveform
ISI
Epileptic Spike
Fast Activity
Period Slow Wave
0
25
Time (ms)
-1
0
1
Time (s)
-2
0
2
Time (s)
-2
0
2
Time (s)
B
Waveform
ISI
Epileptic Spike
Fast Activity
Period Slow Wave
0
25
Time (ms)
-2
0
2
Time (s)
-2
0
2
Time (s)
-2
0
2
Time (s)
C
Waveform
ISI
Epileptic Spike
Periodic Fast Activity
1 ms
0
25
Time (ms)
-1
0
1
Time (s)
-2
0
2
Time (s)
D
RPV (%)
0
1
2
3
4
Baseline Firingrate (Hz)
0
3
6
9
12
Fano Factor
0
0.1
0.2
CV
0.75
1.00
1.25
1.50
1.75
Burst Index
0
0.1
0.2
0.3
0.4
SUA
MUA

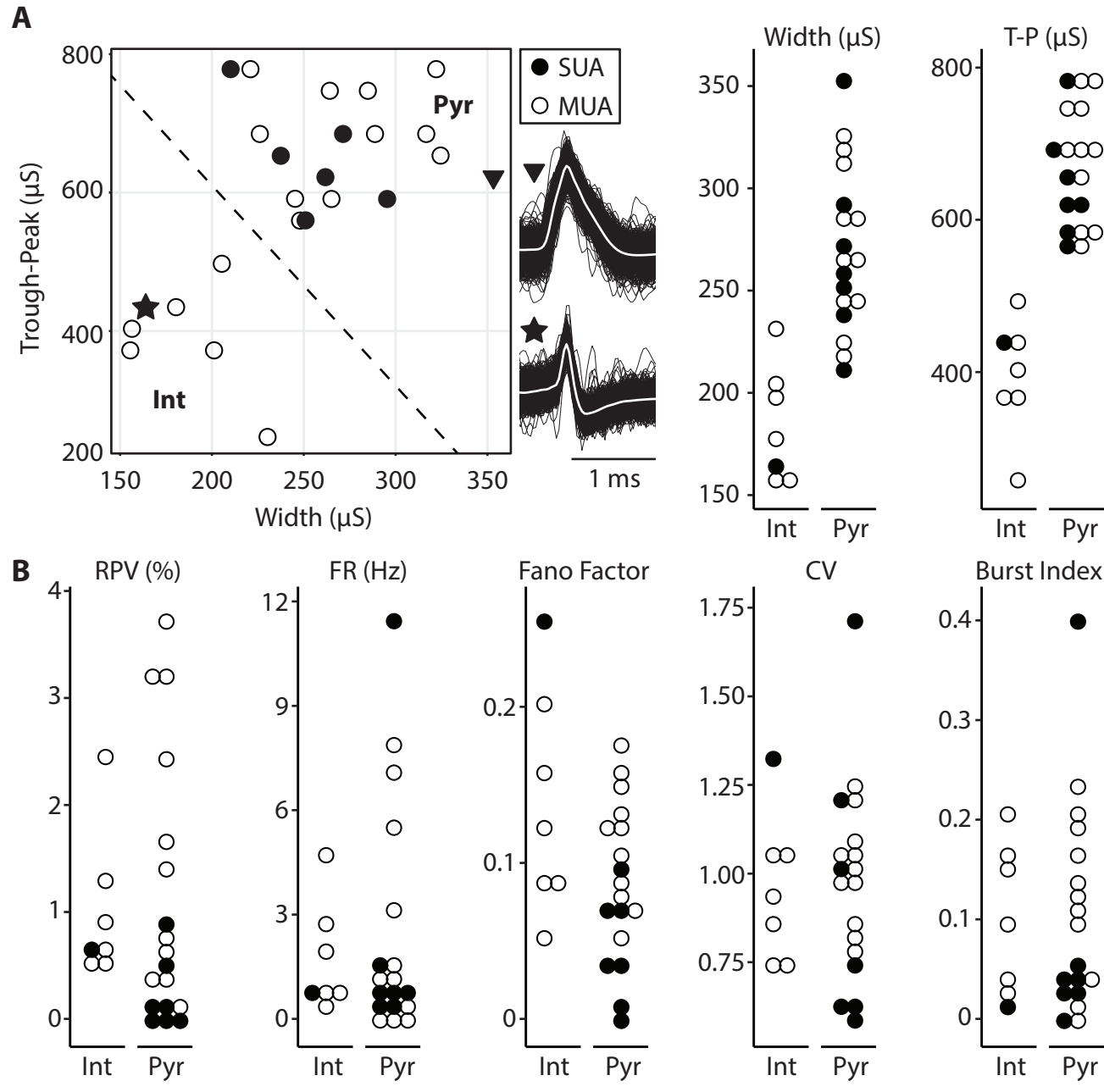
A
Trough-Peak (µS)
Width (µS)
SUA
MUA
Pyr
Int
1 ms
Width (µS)
T-P (µS)
Int
Pyr
B
RPV (%)
FR (Hz)
Fano Factor
CV
Burst Index
Int
Pyr